



Differential Recordings of Local Field Potential: A Genuine Tool to Quantify Functional Connectivity.


Meyer Gabriel¹, Caponcy Julien¹, Paul Salin^{2,3}, Comte Jean-Christophe^{2,3}*

1 Forgetting and Cortical Dynamics Team, Lyon Neuroscience Research Center (CRNL), University Lyon 1, Lyon, France.

2 Biphotonic Microscopy Team, Lyon Neuroscience Research Center (CRNL), University Lyon 1, Lyon, France.

2 3 Forgetting and Cortical Dynamics Team, Lyon Neuroscience Research Center (CRNL), University Lyon 1, Lyon, France, Centre National de la Recherche Scientifique (CNRS), Lyon, France, Institut National de la Santé et de la Recherche Médicale (INSERM), Lyon, France.

 These authors contributed equally to this work.

 Current Address: CNRL UMR5292/U1028, Faculté de Médecine Bâtiment B - 7 rue Guillaume Paradin 69372 LYON Cedex 08.

* jean-christophe.comte@univ-lyon1.fr

Abstract

Local field potential (LFP) recording, is a very useful electrophysiological method to study brain processes. However, this method is criticized to record low frequency activity in a large area of extracellular space potentially contaminated by far sources. Here, we compare ground-referenced (RR) with differential recordings (DR) theoretically and experimentally. We analyze the electrical activity in the rat cortex with these both methods. Compared with the RR, the DR reveals the importance of local phasic oscillatory activities and their coherence between cortical areas. Finally, we argue that *DR* provides an access to a faithful functional connectivity quantization assessment owing to an increase in the signal to noise ratio. This may allow to measure the information propagation delay between two cortical structures.

Author summary

Local field potential (LFP) recording, is a very useful electrophysiological method to study brain processes. However, this method is criticized to record low frequency activity in a large area of extracellular space potentially contaminated by far sources. Here, we compare ground-referenced (RR) with differential recordings (DR) theoretically and experimentally. We analyze the electrical activity in the rat cortex with these both methods. Compared with the RR, the DR reveals the importance of local phasic oscillatory activities and their coherence between cortical areas. Finally, we argue that *DR* provides an access to a faithful functional connectivity quantization assessment owing to an increase in the signal to noise ratio. This may allow to measure the information propagation delay between two cortical structures.

Introduction

LFP recording of cortical structures constitutes a powerful tool to detect functional signatures of cognitive processes. However, several studies have suggested this recording method suffers of major concerns reflecting the activity of distant neuronal populations [1–3]. Thus theta oscillations (6-10Hz) during active wake seems to propagate from the hippocampus to the frontal cortical areas [4] despite these important studies, LFP has revealed important features of cortical organizations (Carandini, Fernandez et al,). For example, cortical slow wave oscillations of NREM sleep which constitute a prominent feature of this vigilance state contribute moderately to coherence between cortical areas. In contrast, weak slow wave oscillations during active wake contribute to a relatively high level of coherence between cortical areas [5, 6]. Single-unit recordings of neurons is a widely used technique in electrophysiological investigations. It is the reason why Local Field Potential (LFP) is still in use. Local field potential signal is mainly owing to the post-synaptic response to the pre-synaptic activity [7–10] and constitutes a natural counter or integrator of the effective action potentials wattering a given cortical region [11–13]. In its classical description LFP appears to be less local than multi-unit activity recordings. Indeed, this recording mode consists to put a single electrode in the investigated cortical region and the second one, in a supposed neutral site. Called monopolar or referential recording (*RR*) mode, the simplicity of this recording configuration is well appropriate to evaluate a global brain state. Unlike single and multi-unit probe, the impedance of the classic electrode of LFP is usually low in order to record the neural activity of a larger area. However, this method may detect activities from distant cortical areas located between the recording and the reference electrode [12–18] a phenomenon called volume conduction. We propose here to compare monopolar or *RR* recording mode to the bipolar or differential one *DR*. Where *DR* consists to set a pair of electrodes in a same cortical area in order to measure the voltage difference between them. The main historical reasons why *RR* is widely sill in use [6, 19] are: 1) the simplicity because of the low number of wires to implant and consequently the brain tissue preservation. 2) The number of available channels to connect to the acquisition devices to record the signals. 3) The method is sufficient to indentify global brain states and oscillations in extracellular space. However, to our knowledge, no study has compared both recording methods in freely moving rats in order to define the best suited configuration to record brain areas activity and quantify their interactions, as well as to extract the guenuine meaning of signals recorded in a specific brain region during a behavioral task [1, 6, 19–27]. The present work has been made possible by our recording configuration described in Method Section.

Thus, the present paper is organized as follow. First, we present the theoretical rational of the paper. After a description of the experimental conditions we experimentally show the difference between the two recording modes through spectral analysis and reveal a new communication frequency band between medial prefrontal cortex *PFC* and the dorsal hippocampus area *CA1*. Before to conclude, we numerically show that the fonctionnal connectivity assesement is strongly impacted by the difference in mode of recordings, explaining why *DR* is much better suited to determine the cortical interactions between cortical areas.

1 Differential and Referential Recordings:

RR recording method consists to record the activity of a cortical region by inserting an electrode in the considered (hot spot) area as well as another electrode located in the reference area (ie skull above the cerebellum, cold spot). In opposition, differential

recordings mode consists to set an electrode pair in a same cortical region. Powerfull signal processing methods such as partial coherence for instance may remove potential contributions of distant neuronal activities [28] and may reduce effect of other distal source. However, as many other cortical areas can potentially generate contaminating signal, it would need an infinity of probes to consider them. Alternatively, to avoid the volume conduction phenomenon is to record cerebral areas through differential recordings consisting in pairs of electrodes in each investigated brain regions (ie differential recording). In this part, we first analyze the theoretical differences between the two modes of LFP recordings.

1.1 What is volume conduction ?

Volume conduction in brain tissue is a well known phenomenon widely observed in conventional local field potential recordings. Volume conduction is a process of current diffusion in a medium. In the brain, the extracellular space contains multiple ionic species. Even if this biological medium is not really homogenous, in order to illustrate and simplify our model we consider it as, linear, homogeneous and isotropic. Considering a punctual current source I diffusing charges in a sphere of radius r , as represented figure (1), in a quasi-static approximation of the Maxwell's equations, the corresponding density of current \vec{J} is given by:

$$\vec{J} = I \vec{u}_r / (4\pi r^2). \quad (1)$$

Using the Ohm law, $\vec{J} = \sigma \vec{E}$ with σ the medium conductivity and \vec{E} the electric field deriving from the potentiel V , ($\vec{E} = -\vec{\nabla}V$). Potential V at a distance r is equal to:

$$V(r) = \frac{I}{4\pi\sigma r}. \quad (2)$$

This expression provides the magnitude of the created potential at a distance r from a given current source I . We observe that this potential decrease nonlinearly with the distance r . From this result, we can easily calculate the potential difference between two electrodes P_1 and P_2 separated by a short distance equal to 2ϵ as represented figure (2). The potential in P_1 and P_2 are expressed as follows:

$$\begin{cases} V_1 = \frac{I}{4\pi\sigma r \sqrt{1 + \frac{\epsilon^2}{r^2} - 2\frac{\epsilon}{r} \cos \alpha}} \\ V_2 = \frac{I}{4\pi\sigma r \sqrt{1 + \frac{\epsilon^2}{r^2} + 2\frac{\epsilon}{r} \cos \alpha}} \end{cases} \quad (3)$$

, and their difference writes,

$$\Delta V = \frac{I}{4\pi\sigma r} \frac{\sqrt{1 + \frac{\epsilon^2}{r^2} - \frac{\epsilon}{r} \cos \alpha} - \sqrt{1 + \frac{\epsilon^2}{r^2} + \frac{\epsilon}{r} \cos \alpha}}{\sqrt{(1 + \frac{\epsilon^2}{r^2})^2 - \frac{\epsilon^2}{r^2} \cos^2 \alpha}}. \quad (4)$$

1.2 Case of a distant source:

In the particular case $r \gg \epsilon$ (i.e. the distance between an electrode and a source is greater than a few ϵ : in practice $\epsilon \sim 50\text{-}200\mu\text{m}$), V_1 and V_2 can be rewritten under

the form:

$$\begin{cases} V_1 = \frac{I}{4\pi\sigma r (1 + \frac{\epsilon}{r} \cos \alpha)} = \frac{I}{4\pi\sigma (r + \delta r)} \\ V_2 = \frac{I}{4\pi\sigma r (1 - \frac{\epsilon}{r} \cos \alpha)} = \frac{I}{4\pi\sigma (r - \delta r)} \end{cases} \quad (5)$$

Setting $\delta r = \epsilon \cos \alpha$, the potential difference between the two electrodes writes:

$$\Delta V_f = 2 \frac{I \delta r}{4\pi r^2}. \quad (6)$$

This result shows that, the potential difference between the two electrodes plays the same role than to push away the source at a distance equal to r^2 , and to damp its intensity by a factor δr of the same order of ϵ . In other words, this fundamental result indicates that differential recording mode removes the contribution of distal sources. Thus, the smaller the distance between electrodes, the smaller the potential difference, and farther a source, and stronger the damping of its intensity. In other words, differential measurement annihilates the contribution of distal sources.

1.3 Case of a local source:

Let us consider now, the case of a local source contribution, that is, a source close to a recording electrodes pair (see fig. 2.b) corresponding to $\epsilon \leq r < 3 \epsilon$. Indeed, because of the distance between the two electrodes, the minimal distance to a source is ϵ , and when $r > 3 \epsilon$, approximations to calculate the potential difference between the two electrodes is similar to the distal source case. As one can observe in figure (2.b) the minimal average distance r (electrodes-source) is equal to ϵ , corresponding to a maximal ratio $\epsilon/r = 1$. The ratio $\epsilon/r < 1/3$ yields the ratio ϵ^2/r^2 negligible and corresponds to the distant source case. Therefore, to condiser the local source case, we have to approximate ϵ to r ($\epsilon \sim r$). Under these conditions, the general expression (3) becomes,

$$\Delta V = \frac{I}{4\pi\sigma\epsilon} \frac{\sqrt{2 - \cos \alpha} - \sqrt{2 + \cos \alpha}}{\sqrt{4 - \cos^2 \alpha}} \simeq \frac{I}{4\pi \sigma \epsilon} \frac{\sqrt{2}}{2} \cos \alpha, \quad (7)$$

that we note ΔV_c .

From these two considerations one can calculate a seperation sources factor Γ , or a Common Mode Rejection Ratio (CMRR):

$$\Gamma = \frac{\Delta V_c}{\Delta V_f} = \frac{\sqrt{2}}{4} \frac{r^2}{\epsilon^2}. \quad (8)$$

This factor summarizes that, farther a source, weaker its contribution, as well as, closer the two electrodes forming the pair, more the local source is visible. The nonlinearity of this ratio, expressed by the square, indicates that the CMRR rapidly change with the modification ratio r/ϵ . For instance, for two arbitrary distances r_1 and r_2 equal to 10ϵ and 100ϵ this ratio go from $\Gamma_1 = 35$ to $\Gamma_2 = 3500$. Finally, we can summarize all of these results by the graphics of figure (3). Indeed, figure (3) represents the potential measured in P_1 and P_2 versus the distance to the source r in normalized units. We note the strong similarity of the potentials when the source is far in comparison with the distance shift ϵ between the two electrodes, leading to a potential difference close to *zero*. The inset zoom figure (3) shows the strong potential difference between the two electrodes when the source is close to the electrodes pair. In summary, we have

shown that differential recording method erases the distal sources contribution and constitutes a practical way to solve the volume conduction problem. In the next part, we assess experimentally the above theoretical predictions as well as we show the genuine difference between referential and differential recordings through different tools such as, spectral analysis, coherence and cross-correlation.

2 Experimental Methods and results:

In order to verify experimentally our theoretical predictions, we performed intra-cerebral recordings in two well known and widely studied areas which are the dorsal *hippocampus* (*CA1*) and the medial prefrontal cortex (*PFC*). The details about the biological preparation is given in annexe A. Figure (3) shows the methodological recordings configuration in which a pair of electrodes is inserted in each brain region of interest, and a *referential* electrode is inserted in the skull just above the cerebellum. A calculation of the difference between the two signals coming from the same cerebral structure allows the differential recording mode (*DR*). This experimental setup has the double interest to access to the two configurations which are referential and differential modes in a same animal and in a same time. In order to avoid any potential artefacts from the animal movements during the wake epoch, we have chosen to focus our attention and analysis about sleep and more specifically during rapid eye movements (REM) sleep (also called paradoxical sleep). REM sleep is characterized by muscle atonia, that is, a very low power signal of the electromyogram (EMG) jointly to a low power signal of the electroencephalogram (EEG) whose spectral energy is mainly located in a narrow band centered around 7 Hz to 8 Hz (θ oscillations). A snippet of a such *EEG* epoch is represented in green figure (4.a). Slow waves sleep also called Non rapid eye movements sleep (NREM) is represented in red figure (4.a). This state is identified by large slow oscillations magnitude accompanied to a low power signal *EMG* but without atonia. Finally, active wake state represented in purple, figure (4.a), presents a low magnitude *EEG* signal close to a gaussian pink colored noise coupled to a strong muscle activity.

2.1 Spectral analysis.

In order to compare the signal differences between the two recording modes *DR* and *RR*, we have performed a spectral analysis by calculating the average power spectrum of the sleep states in *PFC* and *CA1*. Figure (5) shows the power spectra in *RR* mode (blue line) and *DR* mode (red line) in the two investigated brain regions which are *CA1* (top), and *PFC* (bottom), during NREM sleep (left) and REM sleep (right). Spectra result an average of one hundred epochs with a duration of 10 seconds, corresponding to a frequency resolution of 0.1 Hz. The global overview of figure (5) reveals a strong difference between *RR* and *DR* recording modes whatever the brain region and sleep epoch. Beyond the scale factor (~ 10) between the two recording modes, one observes a drastic spectra structure difference. Globally, *DR* spectra present a broader spectral band than *RR*, whatever the brain region and sleep stage. Also, *DR* spectra present a more complex architecture than *RR*. In other words, signals from *DR* and *RR* are qualitatively different even if some parts are similar. Indeed, *RR* is the mix of signals coming from the region of interest as well as signals coming from other asynchronous source regions. Remote asynchronous sources interfere destructively with the local source leading to a rapid decay of the spectrum. *DR* annihilates interfering signals coming from remote sources and then highlights the intrinsic signal of the ROI as we expect and like we have demonstrated in section 1. We can also observe that this fundamental result is state independent. In the new

section, we analyze the *CA1* and *PFC* interplay during REM and NREM sleep in the two recording modes (*DR* and *RR*).

2.2 Coherence and cross-correlation analysis between brain areas.

It is thought that cognitive processes result from information transfer between cortical and subcortical areas [27]. Thus, functional interplay between neuronal populations of different areas remains a major question in neuroscience. Consequently, measurement methods of functional connectivity are crucial to test plausible biological hypotheses. To assess functional connectivity we compared the *DR* and *RR* mode in a same animal in a same time. In this part, we are going to show that *DR* and *RR* are not equivalent, and consequently not the same meaning. Thus, we have performed the coherence calculation between *CA1* and *PFC*. This operation consists to assess the synchrony or phase locking between two signal sources by expression (9), where $X(\nu)$ and $Y(\nu)$ are respectively the Fourier transforms of two signal sources $x(t)$ and $y(t)$. Variable ν corresponds to the frequency, while the star sign designates the complex conjugate operator. Coherence index is a statistical tool similar to correlation index but in the frequency domain instead of time. Thus, we are able to know which spectral component (i.e. frequency) is coherent or phase locked between to cortical areas (cross-spectrum average in the numerator), independently of their magnitude (denominator normalization).

$$C_{XY}(\nu) = \frac{|\overline{X(\nu)Y^*(\nu)}|^2}{\overline{|X(\nu)|^2} \overline{|Y(\nu)|^2}} \quad (9)$$

While *RR* and *DR* power spectra of figure (5) share a some common features, figure (6) shows a large difference of coherence between *RR* (blue line) and *DR* (red line), for *NREM* and *REM*. Indeed, overall, the *RR* coherence spectrum presents a a greater level in comparison to *DR*. The frequency bands for which a peak exist are strongly shifted between the two recording mode *RR* and *DR*. For instance, during *NREM*, the frequency peak is located at 1 *Hz* and 3.5 *Hz* respectively, for *DR* and *RR*. Furthermore, during *REM* sleep, the bigger peak for each recording mode *RR* and *DR* are located at 7 *Hz* and 12 *Hz* respectively. These experimental results, confirm that *DR* and *RR* are two different recording modes with their own physical meaning as we demonstrated theoretically above (sec.1). Whereas *DR* gives access to the intrinsic signal of a given cortical area, that is, the genuine activity of the investigated neural network, coherence is a tool that makes sens to assess the functional connectivity between two cortical region. Consequently, it appears that coherence is strongly dependant of the recording mode. It is also important to note that coherence level is not stationary over time. Indeed, as illustrated in figure (7) we observe that the frequency band (10 *Hz* to 14 *Hz*) presents sporadic bursts of activity in the two recorded cortical structures (*PFC* and *CA1*) at a same time. However, an oscillation at 7 *Hz* persists all along the *REM* episode in *CA1* only. A horizontal projection of this time-frequency diagram provides spectra similar to the figure (5.b) and (5.d), where the average of 7 *Hz* is bigger than the 10 *Hz* to 14 *Hz* in *CA1*, because of the phasic nature of this 10 – 14*Hz* oscillation. This 10 – 14*Hz* oscillation is also observed in th *PFC* during *REM* sleep (figure 7.d). This observation, suggests to explore the dynamics changes of the coherence index. There, we perform the coherence calculation when a 10 – 14 *Hz* events emerge in one of the two investigated brain structures. In order to perform this analyze, we developped a detection routine allowing to isolate the 10 – 14 *Hz* events. The averages calculation in the coherence expression are consequently carried out on the burst events. Figure (8) shows the coherence factor

between *CA1* and *PFC* during *REM* sleep, the traces blue and red correspond respectively to *RR* and *DR* mode, while thin and large traces correspond respectively to the triggering area source (*CA1* or *PFC*). As expected, the choice of the triggering source (*CA1* or *PFC*) does not change the coherence results whatever the recording mode *RR* or *DR*, which first point out the approach robustness. The coherence level in *DR* mode is drastically boosted in comparison with the sliding window average method since the level increases from 0.35 to 0.55, while the coherence level in *RR* mode is drastically reduced from 0.6 to 0.45. Moreover, in order to demonstrate that coherence level obtained with *RR* mode is owing to the volume conduction phenomenon held by the real part of the signal, we have calculated the Imaginary Coherence (IC), which ignore the volume conduction contribution [36]. As shown figure (8), the two majors peaks, the one at very low frequency as well as the one located at 7 Hz (8 left) are strongly damped when we calculate the IC (8 right), meaning that there is no significant phase shift between the cortical areas. Phase shift is owing to a propagating phenomenon, while a zero phase shift is due to a conductive phenomenon. The level of these two peaks is reduced to the basal level of the other frequencies, ending to show that coherence measurement is strongly corrupted in *RR* mode because of the volume condition phenomenon.

An other usefull measurement to understand how brain areas communicate, is the cross-correlation function. This operation is similar to coherence in the temporal domain, and allows to determine the propagation delay between the two investigated brain structures. Propagation direction is determined by the lag sign and the choice of the referential signal (here *PFC*). Figure (9) shows an example of the cross-correlation of two individual burst events (in *DR*) present *CA1* and *PFC*. The maximum peak of magnitude 0.55 is 35 ms lagged, that corresponds to a delay of *PFC* in comparison with *CA1*. In order to compare the ability to measure a delay according to the measurement mode (*RR* versus *DR*), we have performed multiple cross-correlation calculations to construct the lag time probability density function and its corresponding cumulative probability in the two measurement conditions (see fig.9). Figure (9) indicates a null median lag time for the *RR* mode presenting a fuzzy probability density distribution around zero, while a 35 ms median lag time is observable for *DR* mode presenting a genuine identified peak. This lag time value is comparable to the measure obtained by using single cell recording mode [?] which consists to record simultaneously one individual neuron in each structure. This kind of measurements are very complex to perform and allows to ask only one neuron at a time in comparison with LFP which is the superimposition of the effective activity of hundreds neurons reflecting the entire network activity, and consequently avoid to perform multiple single cell recording. In summary, *DR* mode is an efficient way to assess the functional connectivity between brain regions and to identify the communication direction, unlike *RR* mode. The second message is that functionnal connectivity has to be assess when communication between brain region take place in order to avoid the dilution process.

Finally, we have performed numerical simulation in order to show the importance of the signal to noise ratio (SNR) in the coherence index measurement. While the separation source factor or CMRR (8) is equal to $\sqrt{2}/4$ when $\epsilon \sim r$, this one is at once superior to $9\sqrt{2}/4$ when $r > 3\epsilon$. In other words, SNR is about ten times superior in *DR* mode compared to *RR*. Figure (10 right) shows the SNR impact on the coherence level. Indeed, the two arrows indicates the coherence level obtained when SNR^{-1} is equal to 5 and 25 corresponding respectively to the upper and lower graphs of figure (10 left).

3 Discussion

The aim of this paper is to show and explain the differences between the two recording modes, *RR* and *DR*, as well as to examine a way to reduce the contribution of the volume conduction phenomenon in the functional connectivity assessment. Consequently, we have demonstrated theoretically that *RR* and *DR* are two recordings mode with their own properties. We have shown that *RR* is more suitable to define the global state of the brain because of the volume conduction. On the other hand, we have demonstrated that *DR* is able to annihilate the influence of distal sources and is able to probe specific regional activity. Our experimental recordings analysis in the rat show that *DR* yields possible the study of brain areas interplay. Indeed, our coherence analysis shows that *CA1* and *PFC* exhibit a frequency band located between 10 *Hz* and 15 *Hz* not present in the *RR* mode. This result highlights the existence of a such frequency band during *REM* sleep, which is not easily detectable in *RR* mode. This finding constitutes a new functional signature in *REM* sleep. Furthermore, we have observed that oscillations θ in the frequency band (6 *Hz* to 8 *Hz*) present a strong coherence in *RR* mode, while in *DR* mode this band is almost totally extinct, confirming the long distance volume conduction contamination experienced by one electrode. This result, fully justify the use of *DR* mode to investigate the question of cortical areas interactions. Also, we have shown through a time-frequency analysis that communication between *CA1* and *PFC* is sporadic and not continuous as we expect. Using this aspect we have performed a new estimation of the coherence, revealing an increase of this factor in *DR* mode, unlike in *RR* mode. Furthermore, we have computed the cross-correlation synchronized on the burst events in the 10 *Hz* to 15 *Hz* band, and we statistically shown that *PFC* is 30 *ms* late on *CA1* indicating that *CA1* is the transmitter and *PFC* the receptor. Finally, we have performed numerical simulations in order to illustrate the relationship between coherence level and signal to noise ratio. This last result explains clearly the reason why *DR* is better suited to evaluate the interaction between cortical areas than *RR*, since *RR* integrates multiple interfering components. Our study plainly demonstrates the real advantage of *DR* for brain communication understanding and consequently for studying about memory and learning processes. Also, we hope motivate through this work the use of the *DR* mode to explore the cortical communications in future works.

Many electrophysiological recordings tools are available to explore functional brain connectivity. We distinguishes two families with their own properties. The first one is devoted to identify the individual neuron activity, while the second one measure the neuronal field activity, in other the network activity. Single-unit recordings of neurons is a widely used technique in electrophysiology. This recording approach needs sharp and fragile electrode of high impedance ($\gg 1M\Omega$) located close to the cellular body of a neuron, in order to detect the emitted spikes by this one [29,30]. While the interpretation of the measurements is easy when only one neuron participates to the recorded extracellular potential, the task becomes exponentially complex with the number of neurons involved. Indeed, two similar neurons at a same distance to a given recording electrode are difficult to separate from only the electrical perturbation they produce locally. It is the reason why the use of multiple electrodes has been developed such as stereotrode [31] and tetrode [32–35]. All of this recording techniques allow to record and to identify the activity of these neurons with multi-shank electrodes [?]. While it is possible to record one cortical area during a task with such multitrodes the challenge becomes higher when two areas have to be recorded simultaneously and moreover in freely moving animal. Whatever the discipline, the measure principle is to minimize the probe influence on the investigated system. Also, it is important to note that the invasivity increase with the number and the size of electrodes, which may reduce neuronal survival and induce inflammatory

response modifying the measuring medium. Historically, the use of *RR* is justified by two main reasons. The first one is the simplicity because of the weak number of wires to implant and consequently the brain tissue preservation. The second one, is the number of available channels to connect to the acquisition devices to record the signals. Nowadays, these technological limitation are lifted. *RR* is widely still in used [6, 19], despite the advent of the laminar electrodes [7, 8, 17] allowing to reconstruct the current-source density topology and location (iCSD) [15, 19]. However, when the experimental protocol becomes complicated because of the number of cortical sites simultaneously explored in a same animal, it is not surprising to resort to the simplest acquisition mode. Nevertheless, the *RR* and *DR* mode do not provide the same results and consequently the same meaning. To our knowledge, no study has compared both recording methods in freely moving rats, in order to define the best suited configuration to record cortical areas activity and quantify their interactions, as well as to extract the genuine meaning of signals recorded in a specific cortical region during a behavioral task [6, 19–26]. In this study we clarify what is possible to say or not according to the recording mode. Indeed, as we shown above because of the volume conduction phenomenon, the *RR* mode integrates the signals coming from everywhere with a weight inversely proportionnal to the distance. Except in the special case where the signal source is close to the electrode and the distal sources are lows, quickly the sum of distal sources contribution is stronger than the local signal. This phenomenon is relatively interesting to identify global state changes and is widely used in this direction. However, studies used the *RR* mode to quantify the functional connectivity between cortical areas [6, 19]. Although, coherence and cross-correlation differences has been observed between vigilance states, this approach does not measure the genuine functional connectivity between cortical areas and leads to conclusions far from reality if considered as such. While *DR* mode presents a magnitude ten times lower than *RR*, indicating that *RR* mode is not local because of the volume conduction phenomenon as we already said above, *DR* mode presents a cortical area specificity. This is highlighted first, by the spectral structure (5.a and 5.b) in *NREM* and *REM* states for which new spectral bands emerge. Also, this result is strengthen by the coherence analysis which makes emerge a new spectral band of interest during *REM* sleep indicating the existence of spindle waves. Coherence is fundamental to explore the relationship between cortical region in the linear approximation, giving a a fonctionnal connectivity assesement. Indeed, the information transfert from one area to an other one is not a copy-paste. Even if a cortical structure is forwardly and strongly connected to another one, the second structure receives signal from other cortical areas which induces a response to their stimulations. In this simple linear point of view, the fonctionnal connectivity is only sensible to the SNR, that is the power ratio between the signal of interest and the rest, meaning that fonctionnal connectivity is systematically underestimated. In other word, the fonctionnal connectivity obtained in *RR* mode is overestimated and has no communication meaning because of the volume conduction phenomenon, while *DR* presents a specific but systematically under estimated value.

4 Conclusion

5 Annex A

The data used was collected from 5 Dark Agouti male rats (Janvier Labs) aged of 10-15 weeks and weighing between 200-250 grams. After surgery for electrode implanting, they were kept in individual cages in a 12/12h (9am-9pm) light/dark cycle with ad libitum access to food and water. One week after surgery, the rats were introduced in

their recording chamber and plugged for recording. The recording chamber consisted of a 60x60x60cm faradized box with removable container for the litter, so that the rats could be changed daily at 10 am without being unplugged. While in the recording chambers, the animals were exposed to a white noise of 70dB and were also provided with food and water ad libitum. The temperature of the chambers was regulated at 23°C. Once the responses were stabilized, and after at least two days of habituation, baseline recordings, which we used for our analysis, took place during at least 24 hours. The animal care and treatment procedures were in accordance with the regulations of the local (Lyon 1 University CE2A-UCBL 55) and European (2010/63/EU) ethics committee for the use of experimental animals. Every effort was made to minimize the number of animals used and any pain and discomfort occurring during surgical or behavioral procedures. The recording pair of electrodes consisted of two twisted tungsten wires (25 μ m in diameter - California Fine Wire, U.S.A.) de-insulated at the tip along approximately 50 μ m. Muscle activity (EMG) in the neck was recorded with a pair of electrodes that were made by gold plating a small and round solder ball at the de-insulated and hooked tip of a conventional small electric wire. In addition, two 100 μ m diameter stainless steel electrodes were implanted for electrical stimulation in the brain, in order to study the synaptic transmission between the hippocampus and the medial prefrontal cortex and between the CA3 and CA1 areas of the hippocampus. The initial purpose of these recordings, which started in 2014, was to compare, for each sleep state, the synaptic transmission before and after long term potentiation, a cellular mechanism of memory. All these electrodes, along with reference screws, were connected to a custom-made 16 channels analog preamplifier by the EIB-27 connector. The signals were then conveyed via a rotating connector (Plastics One, U.S.A.) to a 16 channel amplifier (AM-Systems, U.S.A.) within which this signal was amplified with a gain of 1000. Signals from the different electrodes were then acquired and digitized at 5kHz by a custom Matlab software (The MathWorks, U.S.A.) driving a NI-6343 acquisition board (National Instruments, U.S.A.) before being stored on a computer.

References

1. Kajikawa and Schroeder. How local is the local field potential? *Neuron*, **72**, pp. 847-858, (2011).
2. Parabucki A., Lampl I., Volume Conduction Coupling of Whiskers-Evoked Cortical LFP in the Mouse olfactory Bulb, *Cell Report*, **21**, pp 919-925, (2017).
3. Lalla L, Pavel E., Rueda O., Jurado-Parras M., Brovelli A., and Robbe D., Local or Not Local: Investigating the Nature of Striatal Theta Oscillations in Behaving Rats, *eNeuro*, **5**, pp 128-145, (2017).
4. Sirota A, Montgomery S, Fujisawa S, Isomura Y. Zugaro M, Buzaki G., Entrainment of neocortical neurons and gamma oscillations by the hippocampal theta rhythm, *Neuron*, **60**, pp 683-697, (2008).
5. Katzner S., Nauhaus I, Benucci A, Bonin V, Ringach DL, Carandini M., Local origin of field potentials in visual cortex, *Neuron* **61** pp 35-41, (2009)
6. Fernandez L., Comte J.C., Le Merre P., Crochet. S., Highly Dynamic Spatiotemporal Organization of Low-Frequency Activities During Behavioral States in the Mouse Cerebral Cortex, **14**, *Cerebral Cortex*, pp 1-19 (2016)
7. Mitzdorf U., Current source density method and application in cat cerebral cortex: investigation of evoked potentials and EEG phenomena. *Physiol. Rev.*, **65**, pp 37-100, (1985).

8. Einevoll G.T., Pettersen K.H., Devor A., Ulbert I., Helgren E. and Dale A.M., Laminar population analysis: estimating firing rates and evoked synaptic activity from multielectrode recordings in rat barrel cortex, *J. Neurophysiol.*, **97**, pp 2174-2190, (2007).
9. Pettersen K.H., Devor A., Ulbert I., Dale A.M., and Einevoll G.T., Current source density estimation based on inversion of electrostatic forward solution: effects of finite extent of neuronal activity and conductivity discontinuities. *J. Neurosci. Methods*, **154**, pp 116-133, (2006).
10. Linden H., Pettersen K.H., Tetzlaff T., Potjans T., Denker M., Diesmann M, Grün S. and Einevoll G.T., Estimating the spatial range of local field potentials in a cortical population model. *BM Neurosci.*, **10** (supplement 1), pp 224, (2009).
11. Nunez P.L. and Srinivasan R., *Electric field of the brain: The neurophysics of EEG*. Oxford University Press. (2006).
12. Kreiman G, Hung C.P., Krakov A., Quiroga R.Q., Poggio T. and DiCarlo J.J., Object selectivity of local field potentials and spikes in the macaque inferior temporal cortex. *Neuron*, **49**, pp 433-445, (2006).
13. Liu J. and Newsome W.T., Local field potential in cortical area MT. Stimulus tuning and behavioral correlations, *J. Neurosci.* **26**, pp 7779-7790, (2006).
14. Leski S., Wojcik D.K., Tereszczuk J., Swiejkowski D.A., Kublik E, and Wrobel A., Inverse current-source density method in 3D : reconstruction fidelity, boundary effects, and influence of distance sources. *Neuroinformatics*, **5**, pp 207-222, (2007).
15. Leski S., Pettersen K.H. Tuntsall B., Einevoll G.T. Gigg J. and Wojcik D.K., Inverse current source density method in two dimensions: inferring neural activation from multielectrode recordings. *Neuroinformatics*, **9**, pp 401-425, (2011).
16. Berens P., Keliris G.A., Ecker A.S. Logothetis N. and Tolias A.S. Comparing the feature selectivity of the gamma-band of the local field potential and the underlying spiking activity in primate visual cortex. *Front. Syst. Neurosci.*, **10**.3389/neuro.06/002.2008, (2008).
17. Pettersen K.H., Hagen E. and Einevoll G.T., Estimation of population firing rates and current source densities from laminar electrode recordings, *J. Comput. Neurosci.*, **24**, pp 291-313, (2008).
18. Linden H., Pettersen K.H. and Einevoll G.T., Intrinsic dendritic filtering gives low-pass power spectra of local field potentials, *J. Comput. Neurosci.*, **29**, pp 423-444, (2010).
19. Sreenivasan V., Esmaili V., Kiritani T., Galan K., Crochet S., Petersen C., Movement initiation signals in mouse whisker motor cortex, *Neuron* **92**, pp 1368-1382 (2016).
20. Logothetis N.K., Kayser C. and Oeltermann A., In vivo measurement of cortical impedance spectrum in mokeys: implications for signal propagation. *Neuron*, **55**, pp 809-823, (2007).

21. Hämäläinen M., Hari R., Ilmoniemi R., Knuutila J. and Lounasmaa O, Magnetoencephalography theory, instrumentation, and applications to noninvasive studies of working human brain, *Rev. Mod. Phys.*,**65**, pp 413-497, (1993).
22. Brette R., Destexhe A., *Handbook of Neuronal Activity Measurement*, Cambridge, ISBN 978-0-521-51622-8, (2012).
23. Bédard C., Kröger H. and Destexhe A., Modeling extra-cellular field potentials and frequency-filtering properties of extracellular space, *Biophys. J.*,**86**, 1829-1842, (2004).
24. Bédard C., Kröger H. and Destexhe A., Does $1/f$ frequency scaling of brain signals reflect self-organized critical states ?, *Phys. Rev. Lett.*,**97**, 118102, (2006).
25. Bédard C., Kröger H. and Destexhe A., Model of low-pass filtering of local field potential in brain tissue, *Phys. Rev. Lett.*,**73**, 0511911, (2006).
26. Vyazovskiy VV, Olcese U, Hanlon EC, Nir Y, Cirelli C, Tononi G (2011). Local sleep in awake rats. *Nature*, 472 (7344), pp. 443–447.
27. Maingret, N. et al . Hippocampo-cortical coupling mediates memory consolidation during sleep. *Nat. Neuroscience*, **19**, pp.959-970, (2016).
28. Buzsáki G., Large scale recording of neuronal ensembles. *Nature Neurosci.*, **7**, pp 446-451,(2004).
29. Gold C.,Henze DA. and Koch C., Using extracellular action potential recordings to constrain compartmental models, *J. Comput. Neurosci.*,**23**, pp 39-58.
30. Gold C.,Henze DA., Koch C. and Buzsáki G., On the origin of the extracellular action potential waveform: a modeling study. *J. Neurophysiol*, **95**, pp 3113-3128 (2006).
31. McNaughton B., O'Keefe J. and Barenz CA., The stereotrode: A new technique for simultaneous isolation of several single units in the central nervous system from multiple unit records, *J. Neurosci. Methods*, **8**, pp 391-397 (1983).
32. Recce M. and O' Keefe J., The tetrode: a new technique for multi-unit extra-cellular recording, *Soc. Neurosci. Abstr.*,**15**, pp 1250, (1989).
33. Wilson M.A. and McNaughton B.L., Dynamics of hippocampal ensemble code for space. *Science*,**261**, pp 1055-1058, (1993).
34. Gray C.M., Maldonado P.E., Wilson M. and McNaughton B., Tetrodes markedly improve the reliability and yield of multiple single-unit isolation from multi-unit recordings in cat striate cortex, *J. Neurosci. Methods*, **63**, pp 43-54,(1995).
35. Jog M.S., Connolly C.I., Kubota Y., Iyengar D.R. Garrido L, Harlan R. and Graybiel A.M.Tetrodes technology: advances in implantable hardware, neuroimaging, and data analysis techniques. *J. Neurosci. Methods*, **117**, pp 141-152, (2002).
36. Sander TH, Bock A, Leistner S, Kuhn A, Trahms L., Coherence and imaginary part of coherency identifies cortico-muscular and cortico-thalamic coupling, *Conf Proc IEEE Eng Med Biol Soc.*, pp 1714-1721, (2010).

Figures Captions

Fig 1. Current source: A current in an homogenous medium yields a current source density diffusing in all the directions. The current density writes: $\vec{J} = \frac{I \vec{u}_r}{4 \pi r^2}$, where r is the distance to the current source and I the current generated at the origine. The Ohm law ($\vec{J} = \sigma \vec{E}$) allows to determine the potential $V = \frac{I}{4 \pi \sigma r}$ created at any distance r .

Fig 2. a) Distal source: A distal source (blue ellipse) release a density of current which gives birth to two remote potentials P_1 and P_2 respectively located at a distance $r - \delta r$ and $r + \delta r$ belonging to the same brain area (red ellipse). This potential are measured by two electrodes spaced from a distance ϵ . b) Local source: A local source (blue ellipse) release a density of current which gives birth to local potentials P_1 and P_2 respectively located at a distance $r - \delta r$ and $r + \delta r$ belonging to the same brain area (red ellipse), where $r \sim 2\epsilon$. This potential are measured by two electrodes spaced from a distance ϵ .

Fig 3. Example of potential measured in P_1 and P_2 versus distance r in normalized units. One notes the strong similitude between P_1 and P_2 when r is big in comparison with the distance shift ϵ of the two electrodes. Also, one observes the strong amplitude difference between potential P_1 and P_2 when the current source is close to the electrodes pair (zoom in figure).

Fig 4. Top: Snippets of typical electroencephalogram (*EEG*) and electromyogram (*EMG*) recordings for the 3 vigilance states, which are wake (Wake→purple), non-rapid eyes movements (NREM→red) sleep, and rapid eyes movements sleep (REM→green). Bottom: Example of hypnogram showing a temporal vigilance states dynamics.

Fig 5. Power spectrum of the two simultaneous recording modes *RR* (blue) and *DR* (red), in *CA1* and *PFC* respectively top and bottom, during NREM (left) sleep and REM sleep (right).

Fig 6. Coherence index between two brain regions (*CA1* and *PFC*) during *NREM* and *REM*, in blue for *RR* and red for *DR*, respectively.

Fig 7. Time-frequency representation of a simultaneous *PFC* (top) and *CA1* (bottom) recording during *REM* sleep, showing occasional large frequency bursts of activity common to the two brain structures and a persistant oscillation at 7 Hz REM sleep θ oscillation, which is the fundamental *REM* sleep signature in *CA1*. Colorbar on the right is the normalized scale color of the time-frequency plot.

Fig 8. Left: Coherence between *CA1* and *PFC* during *REM* sleep for the two recording modes *RR* (blue) and *DR* (red), and the triggering conditions: triggered according to *CA1* thin trace, and triggered according to *PFC* large trace. Right: Imaginary Coherence between *CA1* – *PFC* in *RR* configuration, showing the melt down of the 7 *Hz* peak as well as the very low frequency peak, because of the volume conduction holded by the real part. The 10 *Hz* to 15 *Hz* frequency band stays absent because of the poor signal to noise ratio in *RR* configuration. Inset: vertical zoom of the coherence.

Fig 9. Left: Individual event cross-correlation between *CA1* and *PFC* in *DR* mode, showing a maximum correlation level of 0.55 at a positive lag time of 35 *ms* between the two regions. This positive lag indicates in our case a delay from the *PFC* in comparison with *CA1*. Right: Probability density function (blue) and cumulative probability (red) of cross-correlation peak lag. A zoom on the maximum of the probability density function shows, in referential mode (*ref.*): a null median lag time and a fuzzy probability density function, while in differential mode (*diff*) zoom displays very well indentified peak and median lag time localized to 30 *ms*.

Fig 10. Coherence index vs noise to signal ratio (SNR^{-1}): Left, figures respectively top and bottom are an example of signals used to compute the coherence index for which the coherence is pointed out on the right figure. The coherence calculations have been performed between a pure sine wave (green line) of unit amplitude vs itself added to a noise. The coherence index decreases drastically with SNR^{-1} according to a hyperbolic secant law (red line).

